Highlights

Long-range earthquake energy-release process under locally homogeneous conditions between 2007-2014 at northern Chile

Patricio A. Toledo,Cristián Siegel,Sebastián Riquelme,Raúl Madariaga,Jaime Campos

- We move from a stress release model to a strain release model.
- All events from a seismic catalog are used, i.e. it is not needed to use declustering.
- Strain response depends on scale.

Long-range earthquake energy-release process under locally homogeneous conditions between 2007-2014 at northern Chile

Patricio A. Toledo[a], Cristián Siegel[a,*], Sebastián Riquelme[a,d], Raúl Madariaga[a,c] and Jaime Campos[a,b]

[a]Seismic Risk Program, University of Chile., Blanco Encalada 2002, Santiago, Chile
[b]Geophysics Department, University of Chile, Beauchef 850, Santiago, Chile
[d]Centro Sismológico Nacional, University of Chile, Blanco Encalada 2002 – Casilla #2777, Santiago, Chile
[c]Département de Géologie, Ecole Normale Superieure, PSL University, 75005, Paris, France

ABSTRACT

The seismic cycle in subduction zones comprehends a phenomena of build-up and release of strain, which is punctuated by the occurrence of earthquakes. Nonetheless, the occurrence of earthquakes themselves depends on the relative plate velocity and on lateral heterogeneities that ponderate the energy release. This characteristic is exploited in order to obtain a seismic cycle representation in Northern Chile, using data from the IPOC catalog in the years 2007–2014. We propose and evaluate a scaling relationship for the energy released by earthquakes in a determined scale, depending on the elastic modulus, earthquake displacement and mean stress drop. Displacement, on the other hand, is obtained assuming that the seismicity rate is locally homogeneous and that the averaged regional balance process, which counters tectonic displacement in time due to plates relative velocity with the cumulative sum of earthquake displacements, washes out on the long term. This framework allowed us to obtain a seismic cycle representation between megathrust earthquakes from 2007 and 2014, accounting for a variety of phenomena observed.

1. Introduction

The current seismic-cycle understanding branches into different modeling styles in terms of the existing processes taking place at a given time and location. Two end members are very slow movements, like rock-creep and sudden movements, like regular earthquakes (Ide et al., 2007). Halfway there is a rich group of phenomena like tremors, tsunami-earthquakes and silent-earthquakes not fully incorporated into a single physical framework yet (Avouac, 2015). Likewise important societal problems such as hazard and risk assessment are related to the aforementioned phenomena, thus its understanding constitutes both a fundamental and practical issue. In this study we attempt to understand the build-up and release phenomena using tools from both mechanics and dynamical systems.

Taking advantage of the instrumentation installed at northern Chile, which makes use of both temporary and permanent stations from the National Seismological Center (Barrientos, 2018) and IPOC (GFZ German Research Centre For Geosciences and Institut Des Sciences De L'Univers-Centre National De La Recherche CNRS-INSU, 2006) it has been possible to obtain a well detailed picture of the seismic cycle covering two events with magnitude greater than 7.5 between 2007 and 2014 which allows us to make an unprecedented analysis in terms of the first order information that is recorded, i.e. by seismological catalogs. We attempt to understand the build-up and release phenomena using tools from both mechanics and dynamical systems. Hereafter, in section 1.1 we establish the stochastic processes at work in the crust, in section 1.2 we obtain precise conditions that allow us to parameterize the average deformation that is sustained in the crust as a function of the working scale. Section 1.3 defines the compound process and the regional balance process, the latter defining the state of the crust, thus from a long-term equilibrium condition it is possible to make the connection between seismic coupling and geodetic coupling as a function of the working scale. In section 1.4 the incomplete similarity hypothesis is established for the main study variable which inherits its properties from the fractal distribution of seismicity. In section 2 we review the data used and the main analysis methods. In Section 3 and Section 4 we discuss the main features found and their implications. Among the main elements that naturally appear in this analysis we can mention the intermittency, the very long term deformation associated to visco-elastic movements, the observation of hysteresis and finally we discuss these elements in the regional tectonic context in terms of the segments proposed before from geodetic coupling information.

1.1. Problem setting: stochastic processes within the crust

A deterministic earthquake description generally takes into account the moment release during an observation time-lapse T, however this phenomenon is richer: given the uncertainty in all observable variables a generalization might be obtained considering not only fluctuations derived from instrumental errors but from its full random nature.

Let us fix a typical setting at the west edge of South America as shown in Figure 1. In line with Reid elastic

*Corresponding author: cristian.siegel@uchile.cl
ORCID(s): 0000-0002-0484-0555 (P.A. Toledo); 0000-0001-9562-6812 (C. Siegel); 0000-0002-3953-3504 (S. Riquelme); 0000-0003-2524-9489 (R. Madariaga); 0000-0002-5924-9009 (J. Campos)

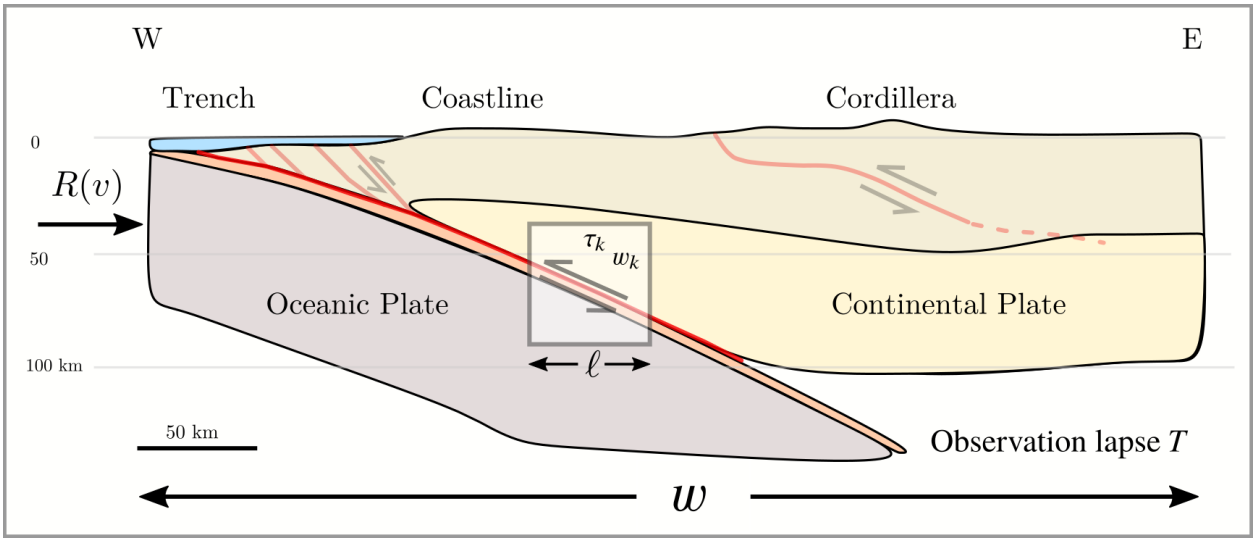

Figure 1: Schematic cross section of a subduction border. A long-term energy injection source R depending on long-term plate velocity v is placed west. As time goes, the Oceanic Plate subduces the Continental Plate creating Trench-Coastline-Cordillera geomorphologies characteristic of a deformation w induced over a time-lapse T. The long-term injected energy is released through earthquakes scattered in a volume with proper length ℓ with interevent-times τ_k marked with displacements w_k, with $k = 1, 2 \ldots$ a point-catalog index. Various stochastic processes representing deformation, timings, build/release cycles might be defined in this setting.

rebound coefficient model, a crust volume with proper length ℓ is loaded at a divergent margin by a long-term energy injection rate R —a function of long-term plate velocity v— creating a trench where an accretionary prism develops by volume contraction (or extension) w with finite strain ℓ/w. This structural setting is referred as a convergent margin characterized by a localized deformation build-up around a damaged zone with banded geometry, called the seismogenic zone. Not far away from the trench, ca. 100 km in South America, a Cordillera region develops by interaction with a buttress and another deformation region growths, now with protracted geometry.

A counting process $\{n(t),\ t \geq 0\}$ might be defined over the seismogenic zone such that its value increases when an earthquake takes place, obviously it is a function of time and it can be considered a continuous time stochastic process:

$$0 = n(0) < n(1) < n(2) < \ldots , \tag{1}$$

so that each moment an earthquake takes place, this count increases one unit and therefore its statistical properties, like the mean number of earthquakes up to a given time t, should be renormalized. An example is shown in Figure 2a. This counting process has various distinguished cases depending on 1) increments independence, that is given time intervals $s_2 < t_2$ and $s_1 < t_1$ the increments $n(s_2) - n(t_2)$ and $n(s_1) - n(t_1)$ can be supposed to be independent random variables 2) increments stationarity, that is given $s < t$, the increment $n(s) - n(t)$ can be supposed to be a function of $s - t$ only and 3) Poisson distribution, that is at a given time-lapse t, the counting random variable can be supposed to be distributed according to:

$$n(t) \sim \frac{\nu^n}{n!} \exp(-\nu) , \tag{2}$$

where ν is a dimensionless rate, in general a time function. When there is a linear time-dependence $\nu(t) = \lambda t$, meaning that the number of events allocated in a time-lapse t increases linearly with the time-lapse. Thus, the mean number of events per time-lapse can be estimated as $\langle n \rangle = \lambda t$. This particular case is called the *homogeneous Poisson process*. When increments are no longer stationary —see Appendix A, the dimensionless rate $\nu(t)$ is non-linear time-dependent, and this case is called the *non-homogeneous Poisson process.*

The occurrence-process $\{t_k,\ k = 1, 2, \ldots\}$ are the discrete times recorded in earthquake point-catalogs when an event happened,

$$0 = t_0 < t_1 < t_2 < \ldots , \tag{3}$$

as seen in Figure 2c. Greater relevance has the interevent-times process $\{\tau_k,\ k = 1, 2, \ldots\}$,

$$\tau_1, \tau_2, \ldots, \tau_k, \ldots , \tag{4}$$

that is the retrograde time difference between events $\tau_k(t) = t_k - t_{k-1}$, with $k = 1, 2, \ldots$, it is generally assumed that all interevent-times are distributed with a known distribution of fixed parameters, that is observed values τ_k are random samples from a unique distribution for all values of k. It is possible to show that if the interevent-times follow an exponential probability law with mean $\langle \tau_k \rangle = 1/\lambda$, independent of k, that is:

$$\tau_k(t) \sim \lambda \exp(-\lambda t) , \tag{5}$$

then the earthquake count $n(t)$ is a homogeneous Poisson process with dimensionless rate $\nu(t) = \lambda t$, this is the so-called classical model linking exponential interevent-times with Poisson counting (Lomnitz-Adler and Lomnitz, 1979).

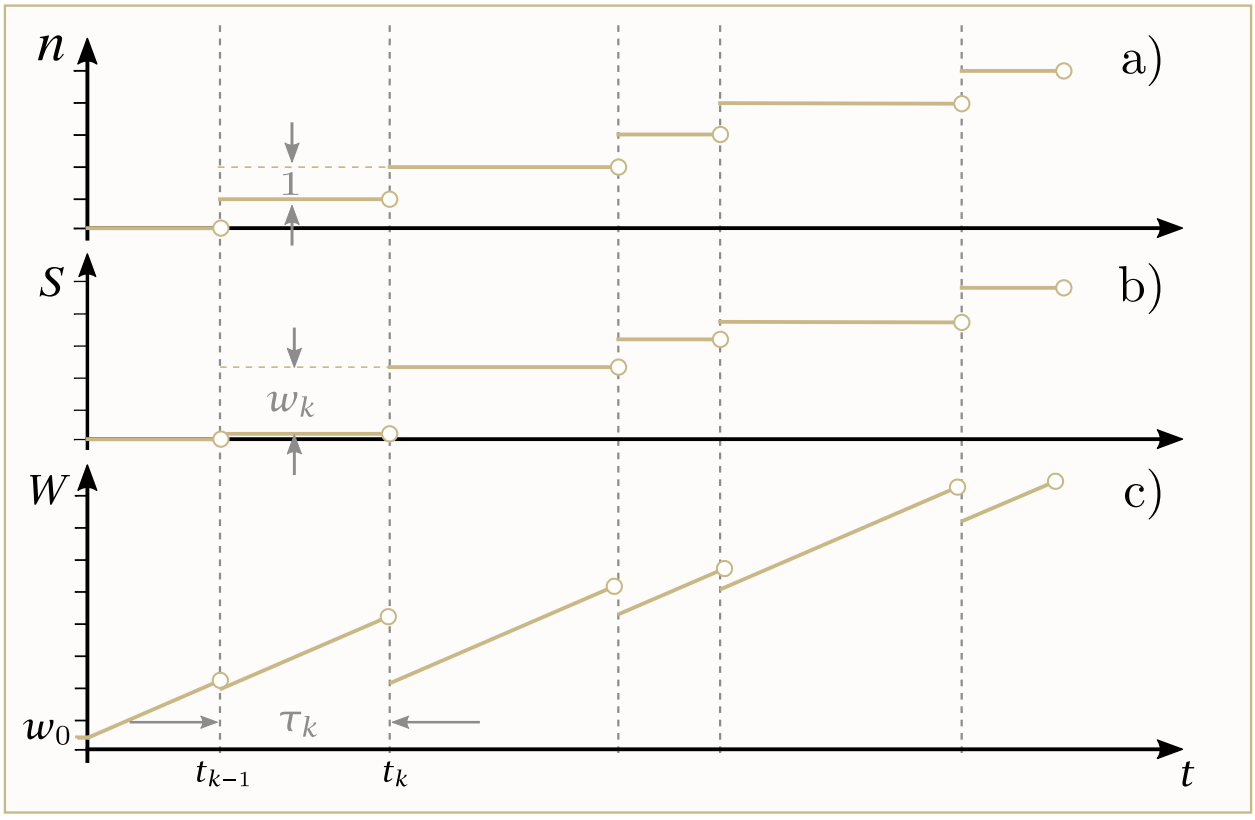

Figure 2: Fundamental stochastic processes in the crust. Over a continuous time variable t events are recorded as points in space-time-magnitude space. Given a geographic volume of interest a subprocess composed of all events within that volume might be described by an event timing stochastic process t_k from where a process τ_k representing retrograde interevent-times marked with a process w_k representing earthquake displacements might be obtained. Three fundamental processes describe the build/release energy cycle process. a) A counting process n such that it increases by one unit each time an earthquake takes place b) A compound process S with the cumulated earthquake displacement sum up to a time n and c) A regional balance process, starting at w_0, increasing like tectonic displacement w with S discounted.

Finally, seismic events taking place at times t_k have magnitudes m_k, from where a discrete energy-release process $\{U_k,\ k = 1, 2, \dots\}$ might be inferred from an energy-magnitude relationship (Kanamori and Anderson, 1975):

$$U_1, U_2, \dots, U_k, \dots, \tag{6}$$

and like interevent-times, we can suppose a given distribution with known parameters. This characteristics make the time-dependent seismicity a *marked process.*

1.2. Locally homogeneous hypothesis

According to Tsuboi (1956) the elastic energy available is located in a volume ℓ^3 capable of sustain a finite strain w_k/ℓ with a surfacic elastic modulus κ, that is the displacement w_k is spread over scale ℓ. This idea is illustrated in Figure 3 left panel. The practical consequence is the introduction of a grid $\mathcal{G}^\ell$ parametric on the proper length ℓ, composed of a set of cells $\mathcal{G}^\ell_{ij}$, where $i, j = 1, \dots$ are indices as illustrated in Figure 3 right panel. Thus, intersecting an earthquake point-catalog $\mathcal{C}$ with $\mathcal{G}^\ell$ induces subcatalogs $\mathcal{C}^\ell_{ij}$ where a hypothesis can be proposed such that each subcatalog is modeled with a locally homogeneous Poisson process.

Under such conditions, let us introduce an equation first posed by Tsuboi (1940):

$$w_k = c\sqrt{U_k}, \tag{7}$$

where c is called the strain-rebound coefficient (Benioff, 1951; Lomnitz, 1966) as it measures the total regional coseismic displacement discontinuity supported by the volume under consideration.

1.3. Long-term behavior

Following Bebbington and Harte (2003) the count process and the coseismic displacement are linked through the *compound process* $\{S(t),\ t \geq 0\}$ representing the cumulated coseismic displacement:

$$S(t) = \begin{cases} \sum_{k=1}^{n(t)} w_k & n(t) > 0; \\ 0 & n(t) = 0, \end{cases} \tag{8}$$

an example is shown in Figure 2b. A regional balance process $\{W(t),\ t \geq 0\}$ might be introduced as the initial displacement w_0 plus the contraction (extension) displacement coming from ridge energy injection $w(t)$ discounting the

cumulated coseismic displacement:

$$W(t) = w_0 + w(t) - \sum_{k=1}^{n(t)} w_k,\ t \geq 0, \tag{9}$$

this continuous time process describes the crust state. The stress release model of Xiaogu and Vere-Jones (1994) considers a time-linear tectonic load $w(t) = vt$, that is:

$$W(t) = w_0 + vt - \sum_{k=1}^{n(t)} w_k,\ t \geq 0, \tag{10}$$

see Figure 2c for an illustration of this process. The time at which the regional balance $W(t)$ reaches zero marks a bifurcation event where the crust dynamics changes qualitatively, from one tectonic system to its inverse, for instance from build-up to releasing.

The total regional balance process $\{W(t),\ t \geq 0\}$ can be used to estimate the strain-rebound coefficient c when interevent-times are exponentially distributed, that is to say there is a locally homogeneous process at work and the tectonic load is time-linear, it can be shown (Mikosch, 2009) that the averaged regional balance process $\langle W \rangle$ can be written as:

$$\langle W \rangle = vt - c\varpi\lambda t, \tag{11}$$

where ϖ is the squared-root energy (Benioff strain) averaged over the long-term. We can obtain a global stability condition for averaged regional balance under the restriction $\lim_{t\to\infty}\langle W \rangle/t = 0$, that is:

$$c = \frac{v}{\varpi\lambda}, \tag{12}$$

at long times. The relation among those parameters and Scholz and Campos (2012) fluxes is direct: $\varpi\lambda$ is the mean seismic flux and the long-term plate velocity v represents the mean tectonic flux per unit coupled-area, see the locally homogeneous fluxes in Figure 3 left panel where the dependence with area is clear. Thus, c represents the seismic coupling χ integrated over the seismically coupled area (Pacheco et al., 1993; McCaffrey, 2008). Note that we could replace v with the dimensionless interface velocity (McCaffrey et al., 2007) as long as the geodetic coupling $\Phi = (v - v_{\text{interface}})/v$ is known, but that requires direct measurements absent in our earthquake point-catalog. Note that $\Phi \simeq 1$ means great influence on aseismic motion (that is, high values of c) and $\Phi \simeq 0$ means great influence on seismic motion (that is, lower values of c). The long-term balance condition (12) can be used to estimate c from seismic moment and long-term plate velocity measurements, once calibrated, we might obtain a drift-free displacement at cell C_{ij}^{ℓ} at the proper length ℓ.

1.4. Elastic rebound under incomplete similarity conditions

As is well known, $\{U_k,\ k = 1, 2, \ldots\}$ is mainly released when a fault works releasing a certain stress-drop $\Delta\sigma$. As

Table 1
Powers of the dimension function in the EL class for each parameter used in text

	U_k	κ	w_k	ℓ	$\Delta\sigma$
E	1	1	0	0	1
L	0	−2	1	1	−3

U_k presents fractal properties let us find the energy signature in the rebound coefficient c, or equivalently on the seismic coupling. Let us us write the relationship:

$$U_k = \varphi\left(\kappa, w_k, \ell, \Delta\sigma\right), \tag{13}$$

with φ a physically meaningful function. The Table 1 lists powers of the dimension function of the aforementioned parameters considering the class of systems of units EL where units of energy and length are used to describe the phenomenon. For instance, surfacic elastic modulus dimensions are $[\kappa] = EL^{-2}$, and stress-drop dimensions are $[\Delta\sigma] = EL^{-3}$.

There are 4 parameters in equation (13), as the class EL has 2 independent units, there are 2 quantities with independent dimensions, let us say κ and w_k, according to dimensional analysis (Sedov, 1993) the relation:

$$\Pi = \phi\left(\Pi_1, \Pi_2\right), \tag{14}$$

can always be written so that Π, Π_1 and Π_2 are dimensionless parameters and ϕ is an invariant function with respect to the group of transformations induced by change of units. In terms of the physical variables the elastic energy U_k can be written as:

$$\frac{U_k}{\kappa w_k^2} = \phi\left(\frac{\ell}{w_k}, \frac{\Delta\sigma}{\kappa w_k^{-1}}\right). \tag{15}$$

The quantity $\Pi = U_k/\kappa w_k^2$, is a dimensionless energy-release. The quantity $\Pi_1 = \ell/w_k$ is a dimensionless length (a finite strain) controlling change of scales available in the crust. Finally, the quantity $\Pi_2 = \Delta\sigma/\kappa w_k^{-1}$ is a dimensionless stress-drop controlling earthquake properties at the source scale. Let us look for an intermediate asymptotic representation (Barenblatt, 2003) in the dimensionless length Π_1, that is:

$$\Pi^* = \phi^*(\Pi_2^*), \tag{16}$$

where $\Pi^* = \Pi/\Pi_1^{\alpha}$ is a renormalized energy-release and $\Pi_2^* = \Pi_2/\Pi_1^{\alpha_2}$ is a renormalized stress-drop. The meaning of equation (16) is that no matter how large or small Π_1 values are, a considerable effect on the dimensionless value of energy and earthquakes source length scales are. The exponents α and α_2 cannot be determined by dimensional arguments, even in principle, and are to be determined by observational data, experiments or numerical modeling. The scaling function ϕ^* is found by a collapse procedure (Houdayer and Hartmann, 2004). Normally an intermediate asymptotic

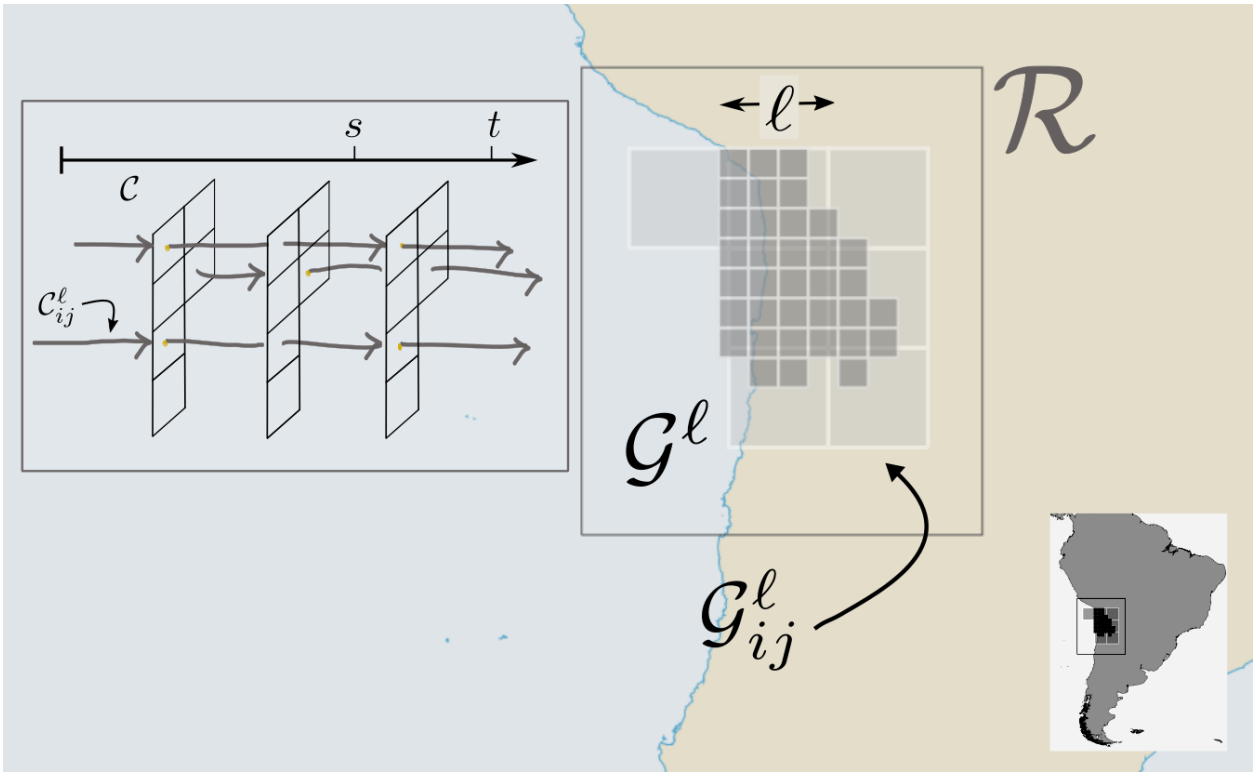

Figure 3: Catalog sketch and griding. An earthquake point-catalog might be intersected with a grid $\mathcal{G}^{\ell}$ covering a region $\mathcal{R}$, so that a marked process where earthquakes occur at instants s and t is induced, thereby creating a subcatalog $\mathcal{C}_{ij}^{\ell}$ for every cell $\mathcal{G}_{ij}^{\ell}$ within the grid interpreted as fluxes. As different proper scales are explored, the process description changes.

solution implies fractality and long-term correlations with anomalous dimensions given by the exponents. Going back to the physical variables we obtain:

$$\frac{1}{\kappa c^2} w_k^{\alpha} \ell^{-\alpha} = \phi^* \left(\frac{\Delta\sigma}{\kappa} w_k^{\alpha_1+1} \ell^{-\alpha_1} \right), \tag{17}$$

so that the fractal character of c is evident, as it decays with positive powers of ℓ, meaning a lacunar support set, and growths with negatives powers values, meaning a invasive support set (Carpinteri and Chiaia, 1997). Same thing can be said about powers of w_k a Gutenberg-Richter law fingerprint.

2. Tectonic framework, data and methods

Let us review our region of interest. As shown in Figure 4a, Nazca advances at 68 mm y^{-1} long-term plate velocity (Norabuena et al., 1998) in N76E direction (Angermann et al., 1999) with respect to South American continent forming a convergent plate tectonics contact. The trace of convergence (trench) is roughly in a north-south direction at the greater bathymetric depths. Under the continent, the subducting plate shows a simple but abrupt morphology (Contreras-Reyes et al., 2012). From 2001 onwards various earthquakes with magnitudes greater than 7.0 have been recorded. Notable examples are the 2007 M_w 7.7 Tocopilla earthquake (Delouis et al., 2009) and the 2014 M_w 8.1 Iquique earthquake (Ruiz et al., 2014).

Figure 4b shows the modern station network managed by IPOC and the Chilean National Seismological Center. We use the earthquake point-catalog published by Sippl et al. (2018) between the years 2007-2014. This catalog contains 101602 events relocated with the double-difference method (Waldhauser and Ellsworth, 2000), which are distributed between 0.01 and 270 km depth, with location errors varying between 1.5 and 15 km depending on hypocenter location. Magnitudes range from 1.3 to 8.1 with cutoff $M_w \simeq 3$. Figure 4c shows the spatial seismic events epicenter distribution. Two latitudinal seismic groups can be observed: seismicity around the coastal zone and seismicity around the inner Andean volcanic arc. The first group corresponds to seismicity associated with shallow subduction mechanics, notoriously denser near 20 and 23° S due to 2014 Iquique earthquake aftershocks. The second group corresponds to seismicity placed up to 270 km depth. According to Hainzl et al. (2019) this catalog has an overall b–value 0.77 ± 0.01 with a mildly positive linear depth dependence. The aftershock rate is reported to follow an Omori exponent near one for magnitudes higher than 6 and considerable variations otherwise, the hypocentral cloud follows a fractal exponent in the range 2.1–2.5.

The main data analysis tool is the griding and box-counting technique (Feder, 2013) as shown in Figure 3 right panel. We used 7 grids having cell lengths ca. 1 up to 1000 km. In Figure 4b the grid with cells ca. 100 km

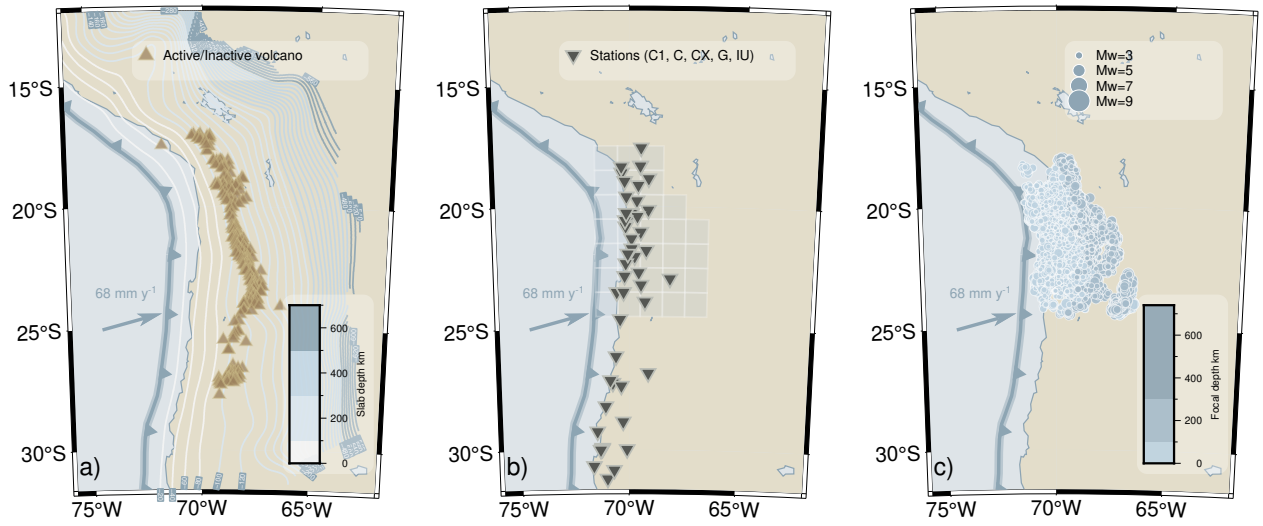

Figure 4: Tectonic, network and earthquake point-catalog context. a) Left, northern Chile plane view. The subduction trace (trench) is roughly axial to coast line. The Nazca plate advances at $68\,\mathrm{mm\,y^{-1}}$ long-term plate velocity. A volcanic arc appears parallel to coastline with a remarkable southern gap correlated with a flatter subduction interface. b) Center, the seismic network being operated (Barrientos, 2018), also a grid with cells covering the region of interest. c) Right, seismicity as published by (Sippl et al., 2018).

is shown. For every subcatalog covering the region — formed after intersecting the earthquake point-catalog with a grid at proper length ℓ— corresponding to every spatial scale explored, mean seismic moment released and unbiased maximum-likelihood mean interevent-times τ are obtained (see tabulated statistics in Toledo, 2021) so approximations for ϖ and λ could be readily obtained, finally equation (12) is used to estimate the rebound coefficient c. Thereupon c scaling is analyzed with equation (16) using data from every cell at every explored proper length ℓ. After a collapsing procedure based on fixed point iteration (Houdayer and Hartmann, 2004) using constrained optimization fit (Branch et al., 1999) surfacic modulus and scaling exponents are calibrated. All estimated parameters are reported with 2σ reverse bootstrap percentiles (Efron and Tibshirani, 1994).

3. Results

3.1. Stochastic processes

In Figure 5 it is possible to see the stochastic processes at the proper length $\ell \simeq 1000\,\mathrm{km}$, which represents the characteristic length covering the whole area of interest and therefore the whole catalog.

The upper panel shows the counting process n together with arrows that mark the magnitude of the seismicity for events greater than 5.5. The 2007 Tocopilla and 2014 Iquique earthquakes are clear, however the counting process appears regular at this scale, there is no appreciable detail of what happens between these earthquakes. The middle panel shows the compound process S obtained after imposing the equilibrium condition (12) to estimate the rebound coefficient.

For these data $c = 4 \times 10^{-15}\,\mathrm{mJ}^{-1/2}$ using the long-term plate velocity already mentioned. It is possible to observe those moments in which this geographic zone presents a deficit/surplus in S with respect to the linear tectonic load as time goes. Before the 2007 Tocopilla earthquake there was a marked deficit followed by a period of surplus covering the entire year 2008. Subsequently, the compound process S grows during 2009 taking off in 2010 and 2011 to undergo another takeoff event during 2012 and 2013 that starts a period of high deformation associated with the preparation phase of the 2014 Iquique earthquake (Ruiz et al., 2014) which, according to this graph, lasts 2 months. After the 2014 Iquique earthquake there is a period in which there is a balance with respect to the linear tectonic load.

In the lower panel it is possible to observe the regional balance process W. Here we can get more clarity regarding the stages already mentioned. The events of 2007 and 2014 are clearly represented as well as the build-up and release phenomena. The 2007 event build-up phenomenon is observed partially, however there are two previous events in February-March and August-September that occur for always positive values W with a release rate of $24\,\mathrm{mmy}^{-1}$ ($\Phi = 35\%$), the strain-drop produced by the 2007 earthquake is followed by a period of visco-elastic relaxation with negative values of W that lasts until January of 2008 that is to say 5 months, later it grows linearly at $16\,\mathrm{mmy}^{-1}$ ($\Phi = 24\%$) release rate for 23 months. From here on it is possible to observe great complexity in the build-up phenomenon. The February 27 2010 Maule earthquake (Vigny et al., 2011) appears notable, since it begins a period of complex build-up and release with a marked detachment from the global drift. It has already been documented that the 2010 earthquake triggered elastoplastic deformation before the 2015 Illapel earthquake (Ruiz et al., 2016), for further background

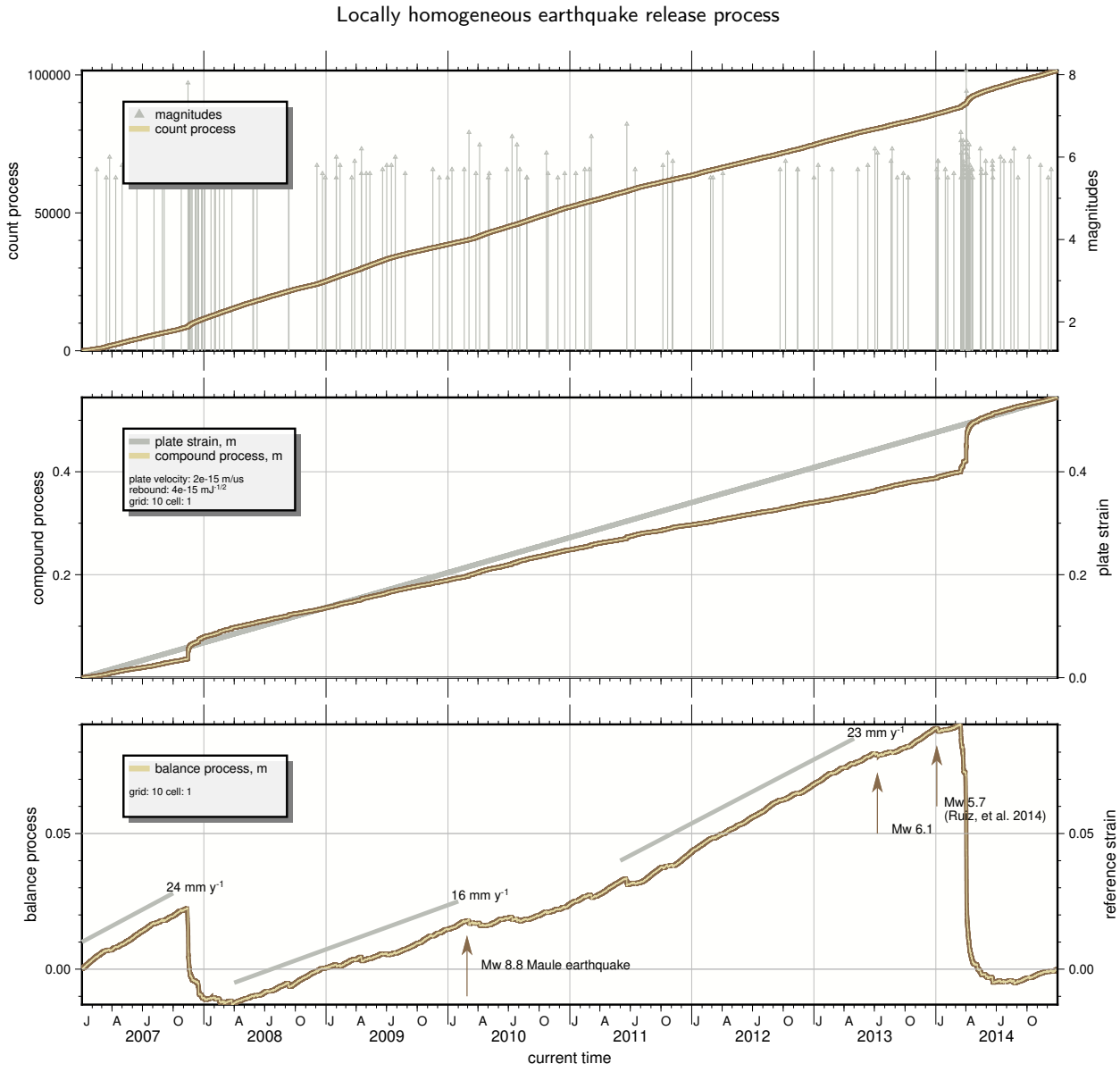

Figure 5: The fundamental processes at the regional scale. a) Upper panel, the counting process n from zero at January 2007 up to 100000 events by December 2014. Arrows show events with magnitudes m_k greater than 5.5, note 2007 M_w 7.7 Tocopilla earthquake and 2014 M_w 8.1 Iquique earthquake. b) Middle panel, the compound process S calibrated with rebound coefficient $c = 3.81 \times 10^{-15}\,\mathrm{m\,J^{-1/2}}$. Also, the linear tectonic plate cumulated displacement $w(t) = v\,t$ is shown considering a long-term plate velocity $v = 68\,\mathrm{mm\,y^{-1}}$. c) Lower panel, the regional balance process W shows a nearly constant build-up until 2007 Tocopilla earthquake, a sudden decrease followed by a relaxation period (ca. 15 months) then a new build-up with an initial lower rate that appears to show an complex acceleration/deceleration ending at 2014 Iquique earthquake again followed by a relaxation period (5 months). The upper yield threshold is very different considering the two mainshocks recorded. The 2014 Iquique earthquake yield threshold ca. 3 times greater than Tocopilla's. Though lower resistance balance is again different, the difference is smaller. Linear long-term rates are indicated. Also three important earthquake dates are marked with arrows.

on both earthquakes see also Ruiz and Madariaga (2018). In this case there would be a clear visco-elastic response ca. 1600 km away that lasts 16 months. Subsequently there is a build-up stage at 23 $\mathrm{mmy^{-1}}$ rate ($\Phi \simeq 24\%$) culminating in two important dates. The July 10, 2013 M_w 6.1 event at 69.5° W, 19.4° S, 116 km depth and the January 4, 2014 M_w 5.7 already reported by Ruiz et al. (2014) as the start of the 2014 Iquique earthquake preparation phase. After the 2014 earthquake, equilibrium is reached with a relaxation period equal to the 2007 Tocopilla earthquake ending in August 2014 that is 5 months. There is a difference in the yield strain for both events, $W = 0.025\,\mathrm{m}$ in a case and $W = 0.09\,\mathrm{m}$ in the other, however the resistance —i.e. the value for which the free-relaxation ends— also presents different values, but the differences are minor.

Let us look at the behavior of the processes ensemble. In Figure 6 it is possible to observe both the compound process and the regional balance process. This time we illustrate samples for grids with proper length $\ell = 100\,\mathrm{m}$ considering a rebound coefficient $c = 4 \times 10^{13}\,\mathrm{m\,J^{-1/2}}$ due scaled. This

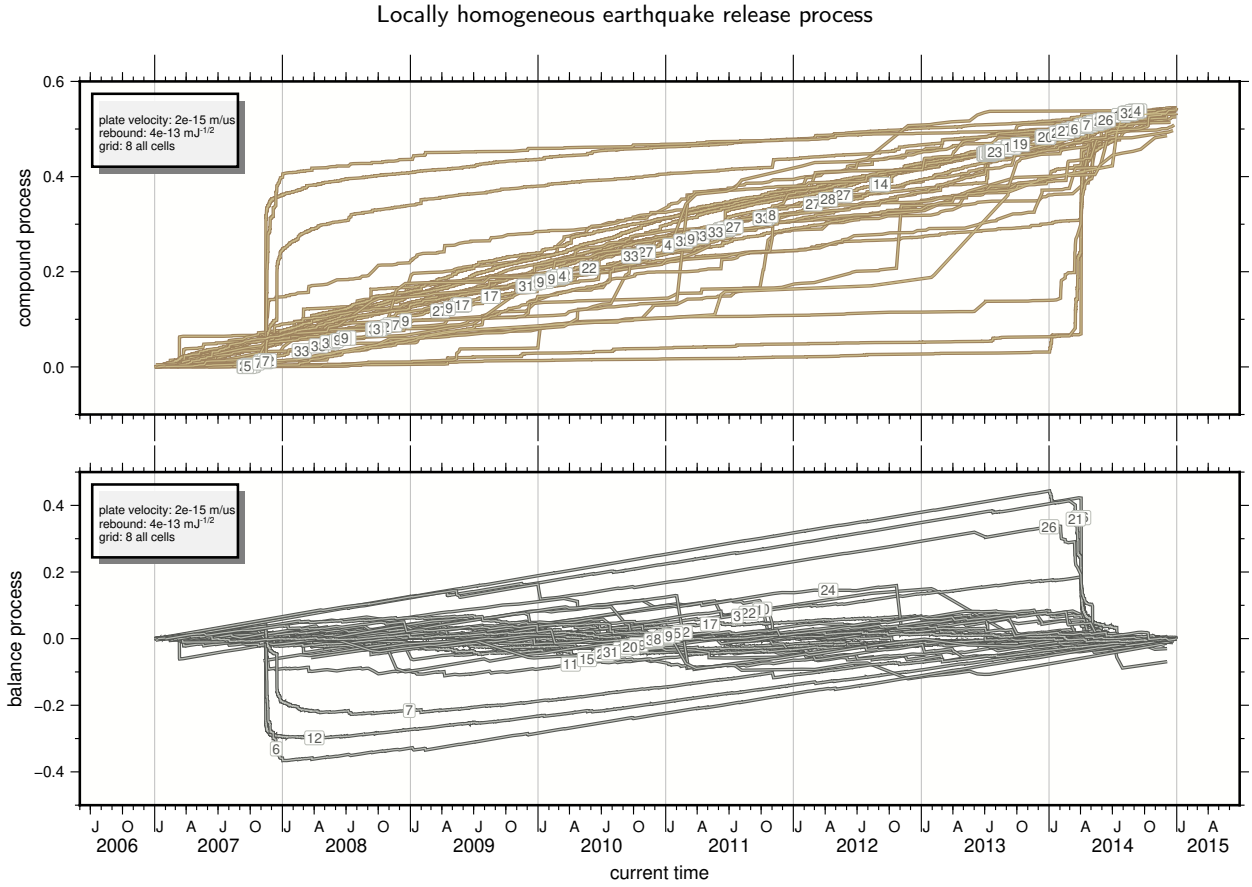

Figure 6: Compound and balance subprocesses found after intersection with a grid with 100 km proper length cells as show in Figure 4 middle panel. Labels indicates cell. In addition to 2007 Tocopilla and 2014 Iquique earthquakes, different processes for different cells show different behaviors but closer cells show similar trends revealing space correlations. At this scale, yield threshold differences are reduced, an effect of the declustering nature of the box-counting methodology embedded in rebound coefficient calculations. The sampled processes cyclic character resembles a hysteresis loop.

happens because by imposing a grid, subcatalogs are induced, one for each cell, and these subcatalogs have different inter-event times and different released moments, which means different rebound coefficient and seismic coupling. This should make it clear that c is not a property of the medium, since it has a strong scale dependency. In both panels it is possible to appreciate the 2007 Tocopilla and 2014 Iquique earthquakes. Each cell studied has a different behavior, however there are spatial similarities, for example cells 6, 12 and 7 suffer from the marked release phenomenon of the 2007 Tocopilla earthquake while cells 26, 21 and 16 sense the 2014 Iquique earthquake, which is clear evidence of spatial correlation between cells and earthquake interaction. More important is the quasi-cyclical nature of the phenomenon, which, due to local variations, translates into hysteresis, that is, a phase difference for each cell as they interact in the same large-scale cycle, therefore not all cells are synchronized, some are at build-up and some are at releasing stages.

3.2. Rebound fractal properties

In Figure 7 a situation where the collapsing procedure is successful is illustrated (see also Appendix B). In this case from a seed with values $\alpha = -2.5$, $\alpha_1 = -2.5$ and $\kappa = 1 \times 10^{26}\,\mathrm{Jm}^{-2}$ fixed-point iterations converge to exponents $\alpha = -1.19^{+0.04}_{-0.06}$, $\alpha_1 = -3.25^{+0.03}_{-0.03}$ and surfacic elastic modulus $\kappa = 1.18^{+0.01}_{-0.01} \times 10^{26}\,\mathrm{Jm}^{-2}$. There is considerable scatter, however it is possible to see similar behavior across 12 orders of magnitude, so it is possible to rescale the values for the renormalized variables in terms of inter-event times, magnitudes and spatial scale. In practice the rescaling means that the rebound coefficient has a lacunar fractal support set that is similar to a Koch curve, see also Figure 8.

Finally, let us analyze the rebound coefficient spatial distribution. In Figure 8 it is possible to see a map for the grid that has proper length $\ell = 10$km. It is important to note that high rebound coefficient values mean $\varpi\lambda \ll v$ that is, the seismic activity goes well below the tectonic load (coupled scenario) and on the contrary low rebound coefficient values mean seismic activity goes well above the tectonic load (decoupled scenario). It is interesting to note three zones previously identified in terms of geodesic coupling Φ by Métois et al. (2013): off the coast around 20° S the Camarones segment, off the coast near 23° S the Loa segment and between 21° S and 23° S the Iquique intersegment. Additionally we can highlight an elongated strip at 70° W from 18° to 24° S that correlates with intermediate-depth seismic activity (Sippl et al., 2018) bounded by 40 km

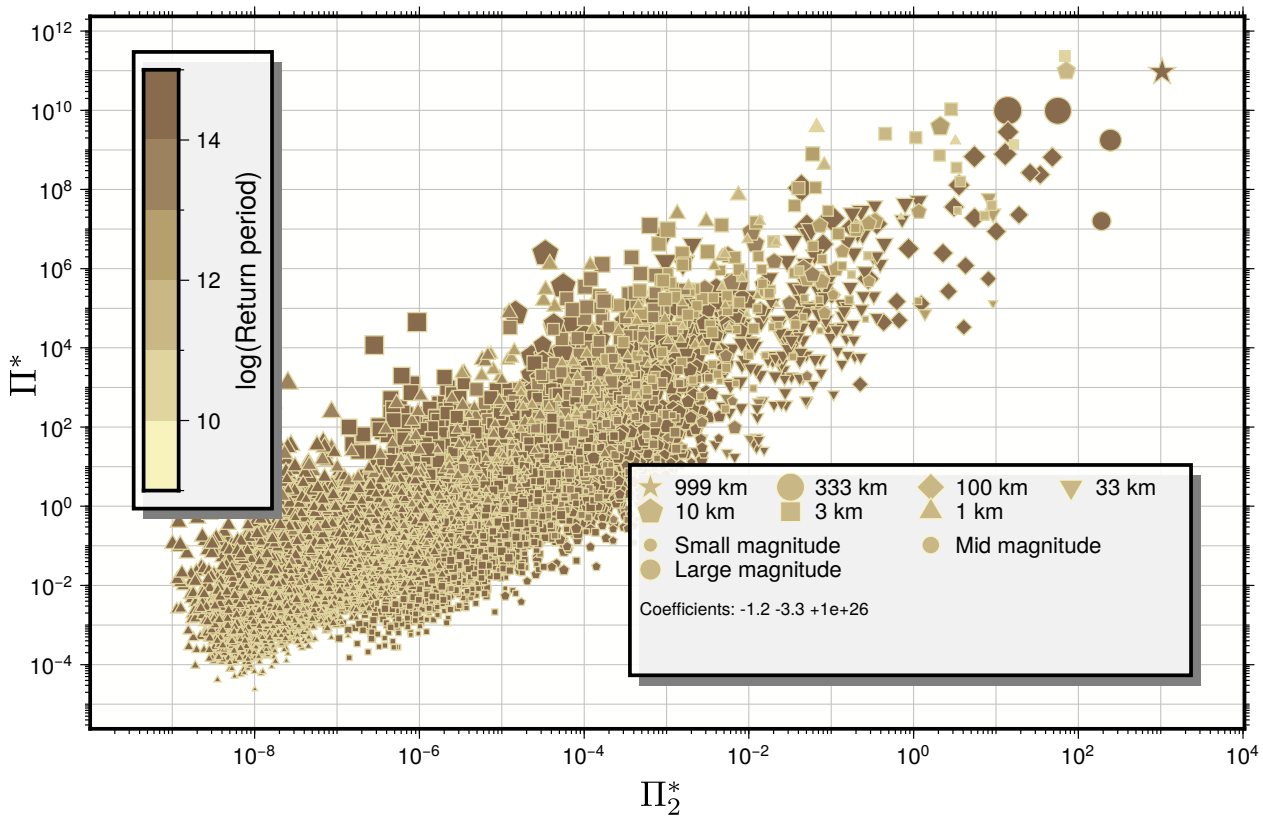

Figure 7: Collapsed renormalized energy versus renormalized stress drops. The scaling function ϕ^* shows a power law albeit with considerable scatter. With rebound coefficient estimated at every explored grid, exponents α, α_1 and surfacic modulus κ might be inverted when ϕ^* is near a fixed-point found through a collapsing procedure. Exponents are $\alpha = -1.19$, $\alpha_1 = -3.25$ and $\kappa = 1.18 \times 10^{26}\,\mathrm{Jm}^{-2}$.

and 60 km plate depth isobaths. Parallel to this, around the 100 km isobath there is a low rebound coefficient zone correlated with deep seismicity under the Volcanic Arc. Finally there is a compact zone at 67° W between 24° and 25° S around 180 km isobath which correlates with deep seismic activity under the Andean Plateau (Valenzuela-Malebrán et al., 2022).

4. Discusion

Stochastic conditions. When statistical conditions are imposed on occurrence times in catalogs, it is usual to resort to exponential inter-event times (Ferraes, 1967). In the case of Probabilistic Seismic Hazard Assessment, for example, a temporal declustering methodology must be introduced due to deviations normally found (e.g. Poulos et al., 2019). In our case, we have relaxed the global exponential interevent-times hypothesis by requesting that n be distributed only locally as a Poisson process, which allows us to estimate the seismic rate λ from the inter-event times in a cell of proper length ℓ. Again, due to the natural declustering introduced by cell length threshold (Janićević et al., 2016) the variability can be recovered by analyzing the dependency with the proper length ℓ. That is, there is a tension between the locality of the interevent-time process and the spatial correlations that are captured in the explicit dependence of the rebound coefficient on the coupled-area $\sim \ell^2$. The existence of a memoryless process also enters into tension with long-term behavior. By imposing a condition for long times in the regional balance process, it happens that the natural drift of the counting process disappears, which gives a physically consistent picture with other relevant observations, let us say GPS, which has a long history in northern Andes research (Ruegg et al., 1996; Chlieh et al., 2004; Métois et al., 2013).

The Rebound coefficient posses a fractal character due to the explicit dependence on proper length ℓ, which appears when locally homogeneity hypothesis was imposed, it is not trivial the form that this dependence on the main parameter studied, which is the rebound coefficient c, therefore the incomplete similarity hypothesis must be taken with care, mainly due to the W process shape, which although it presents spatial correlations (assimilated to a hysteresis cycle in Figure 6) is not clear to have self-similar behavior. Although Π^* has a power-law scaling it is clear that there is also a large dispersion, that is, there is a family of exponents capable of solving the situation. This dispersion is related to the intermittence phenomenon (Frisch and Parisi, 1980) and its multifractal character (Hirata and Imoto, 1991; Hooge et al., 1994). Multifractality has already been observed in the area by Comte et al. (1999) and Pastén and Comte (2014) so it is necessary to further research this aspect, especially

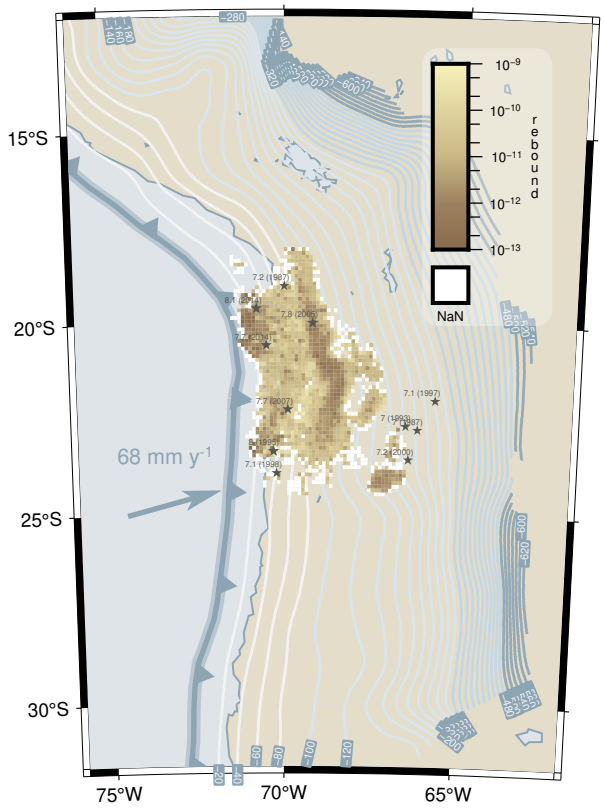

Figure 8: Rebound coefficient map, in $mJ^{-1/2}$. After intersection with a 10 km proper length grid, for each subcatalog produced a single rebound coefficient might be calibrated using equation (12) characteristic of the regional balance and compound processes. A higher rebound coefficient means smaller values of released energy. At 20° S coast a low rebound coefficient patch correlates with 2014 Iquique earthquake epicenter, same thing with 2007 Tocopilla earthquake epicenter near 23° S. A elongated low rebound coefficient strip around 70° W between 18° S and 24° S is clearly seen, correlated with intermediate depth seismicity. A compact patch at 67° W between 24° and 25° S correlates with deep seismicity under Andean Altiplano. The coastal region between 21° S and 23° S shows high coupling values. Stars mark earthquakes recently recorded with magnitudes larger than 7.7 (U.S. Geological Survey, 2021).

it is necessary to solve the mechanism that gives rise to the intermittency, which leads us to next point.

Intermittence. This is a phenomenon observed in nonlinear systems, it is common in those with many activated degrees of freedom, corresponds to the sudden release of energy separated by moments of calm. There are several mechanisms associated with control parameter bifurcations (see Scott, 2006). It has been observed in turbulence (Meneveau and Sreenivasan, 1991) and also in seismicity, both in catalogs (Bottiglieri and Godano, 2007; Telesca et al., 2001) as in automata (Abe and Kato, 2014). According to the model of Benzi et al. (2022), it is characterized by a laminar stage where energy increases proportional to time (calm and build-up phases) that mutate to an avalanche stage where energy decreases in (intermittent) intervals proportional to interevent times powers (burst and release phases) with size distributions as powers too. In Figure 5 the laminar stage is clear at the indicated scale and corresponds to the periods where the tectonic load is linear, some events occur on a smaller scale and others on an intermediate scale, 2014 Iquique earthquake precursors fall into the latter category: they are small enough to belong to the laminar stage and large enough to be observed. In this same sense, we can associate the occurrence of slow slip phenomena (Obara and Kato, 2016) to the laminar stage and fast slip phenomena to the avalanche stage that presents power-law interevent times (see Fig.2 in Rogers and Dragert, 2003, and compare Figure 5 here).

Hysteresis. The yield strain difference between 2007 Tocopilla and 2014 Iquique earthquakes observed in Figure 5 points to the slip-predictability model of Shimazaki and Nakata (1980) which is precisely the model used by Pacheco et al. (1993) to estimate seismic coupling χ, however we must emphasize the appreciable difference in resistance — lower limit of W — long underestimated. A hybrid model may be the best option, but further analysis is needed.

Energy dissipation. The existence of a hysteresis loop means that it is possible to calculate the rate of dissipated energy $\epsilon(t)$ from these observations, which is closely associated with the intermittency phenomenon through tectonic loading:

$$\frac{dW}{dt} \simeq R - \epsilon(t), \tag{18}$$

see Benzi et al. (2022). This is a line that needs to be addressed. The implications for hazard estimation are important: having slowly decaying correlations in both time and space improves the ability to identify variables that allow the occurrence of large events to be approximated from smaller event data, but having a long linear loading period with no appreciable energy release is a much better scenario for hazard estimation. There is evidence that the location where earthquakes occur and their typology (Obara and Kato, 2016) is related, so Figure 8 can better illustrate the occurrence of these phenomena since the rebound coefficient c is associated with the intermittency rate and its own regimes (laminar and avalanches).

Seismotectonics. Finally, we can say that off the coast of the Camarones segment the rebound coefficient is low, that is, it is a scenario where $\varpi\lambda \gg v$, consistent with the relaxation after the 2014 Iquique earthquake. In the Loa segment, the rebound coefficient is similarly low, this time associated with the 2007 Tocopilla earthquake post-seismic stage. The Iquique intersegment presents a higher rebound coefficient than the neighboring segments, which means accumulation of energy proportional to time. The intersegment has not suffered earthquakes of magnitude greater than 7.7 since 1877 (Vigny and Klein, 2022), additionally in Figure 8 it is possible to appreciate the epicenters of events with magnitude greater than 7.7 recently recorded in the global catalog (U.S. Geological Survey, 2021), it can be seen that the rim suffered an aftershock in 2014 (Ruiz et al., 2014) around

the 30 km isobath and that the 2007 Tocopilla poearthquake is at the other extreme. In this intersegment Ruiz et al. (2014) infers the occurrence of a slow earthquake prior to the 2014 Iquique earthquake, according to our analysis, here the regional balance process W would be consistent with slow deformation. In the elongated strip towards the Cordillera between 18° S and 24° S there is also a seismicity deficit. In this case, the geodesy models lose considerable resolution, according to what we interpret, W would have linear growth. Subparallel is the strip related to intermediate depth seismicity around 100 km that has low rebound coefficient values, that is, $\varpi\lambda \gg \upsilon$, or seismic activity above tectonic load. It is in this sector that the M_w 6.1 event is located, which marks the end of the period of linear growth prior to the 2014 Iquique earthquake, so it is interesting to understand the relationship of this deep activity with the upper area (Jara et al., 2017). Finally, the compact patch associated with deep activity at approximately 200 km studied by Valenzuela-Malebrán et al. (2022) has intense seismic activity. In these last two cases, the tectonic situation is that the long-term plate velocity υ is no longer the most relevant variable, and other factors, mainly rheology, may come into play.

5. Conclusions

The seismic-cycle in a subduction zone is a complex phenomena which has as its more clear manifestations individual earthquakes. Although earthquakes are fundamentally extended sources given they are inferred to be material ruptures, most of then can be considered as points in space. Nevertheless, in the temporal dimension, because they are dependent of the plate convergence velocity, it is less clear that they can be considered as point processes. Then, when considering this plate velocity in the balance analysis and assuming the apparent contradiction of a local homogeneous stochastic process, along and upscaling considering a coarse-graining with cells that can host one small event up to a cell with size reminiscent of the whole seismogenic thickness- is it possible to get a picture that make sense of the whole seismic-cycle. This picture posses emergent properties not available before from purely seismic events, but that are more and more frequently made available from geodetic and satellite observations. In overall it comes from the intermediate asymptotics representation, which has been useful to conceal seismicity analysis as a stochastic point process with the diversity of reported phenomena such that it can be possible to integrate them in a single framework.

References

S. Ide, G. C. Beroza, D. R. Shelly, T. Uchide, A scaling law for slow earthquakes, Nature 447 (2007) 76–79.

J.-P. Avouac, From geodetic imaging of seismic and aseismic fault slip to dynamic modeling of the seismic cycle, Annual Review of Earth and Planetary Sciences 43 (2015) 233–271.

S. Barrientos, The seismic network of Chile, Seismological Research Letters 89 (2018) 467–474.

GFZ German Research Centre For Geosciences, Institut Des Sciences De L'Univers-Centre National De La Recherche CNRS-INSU, Ipoc seismic network, 2006. URL: http://geofon.gfz-potsdam.de/doi/network/CX. doi:10.14470/PK615318.

J. Lomnitz-Adler, C. Lomnitz, A modified form of the gutenberg-richter magnitude-frequency relation, Bulletin of the Seismological Society of America 69 (1979) 1209–1214.

H. Kanamori, D. L. Anderson, Theoretical basis of some empirical relations in seismology, Bulletin of the seismological society of America 65 (1975) 1073–1095.

C. Tsuboi, Earthquake energy, earthquake volume, aftershock area, and strength of the Earth's crust, Journal of Physics of the Earth 4 (1956) 63–66.

C. Tsuboi, Isostasy and maximum earthquake energy, Proceedings of the Imperial Academy 16 (1940) 449–454.

H. Benioff, Earthquakes and rock creep: (Part I: Creep characteristics of rocks and the origin of aftershocks), Bulletin of the Seismological Society of America 41 (1951) 31–62.

C. Lomnitz, Statistical prediction of earthquakes, Reviews of Geophysics 4 (1966) 377–393.

M. Bebbington, D. Harte, The linked stress release model for spatio-temporal seismicity: formulations, procedures and applications, Geophysical Journal International 154 (2003) 925–946.

Z. Xiaogu, D. Vere-Jones, Further applications of the stochastic stress release model to historical earthquake data, Tectonophysics 229 (1994) 101–121.

T. Mikosch, Non-Life Insurance Mathematics: An Introduction with the Poisson Processes, Springer Verlag, Berlin, Heidelberg, 2009.

C. H. Scholz, J. Campos, The seismic coupling of subduction zones revisited, Journal of Geophysical Research: Solid Earth 117 (2012).

J. F. Pacheco, L. R. Sykes, C. H. Scholz, Nature of seismic coupling along simple plate boundaries of the subduction type, Journal of Geophysical Research: Solid Earth 98 (1993) 14133–14159.

R. McCaffrey, Global frequency of magnitude 9 earthquakes, Geology 36 (2008) 263–266.

R. McCaffrey, A. I. Qamar, R. W. King, R. Wells, G. Khazaradze, C. A. Williams, C. W. Stevens, J. J. Vollick, P. C. Zwick, Fault locking, block rotation and crustal deformation in the Pacific Northwest, Geophysical Journal International 169 (2007) 1315–1340.

L. I. Sedov, Similarity and dimensional methods in mechanics, CRC press, 1993.

G. I. Barenblatt, Scaling, Cambridge Texts in Applied Mathematics, Cambridge University Press, 2003. doi:10.1017/CBO9780511814921.

J. Houdayer, A. K. Hartmann, Low-temperature behavior of two-dimensional Gaussian Ising spin glasses, Physical Review B 70 (2004) 014418.

A. Carpinteri, B. Chiaia, Multifractal scaling laws in the breaking behaviour of disordered materials, Chaos, Solitons & Fractals 8 (1997) 135–150.

E. Norabuena, L. Leffler-Griffin, A. Mao, T. Dixon, S. Stein, I. S. Sacks, L. Ocola, M. Ellis, Space Geodetic Observations of Nazca-South America Convergence Across the Central Andes, Science 279 (1998) 358–362.

D. Angermann, J. Klotz, C. Reigber, Space-geodetic estimation of the Nazca-South America Euler vector, Earth and Planetary Science Letters 171 (1999) 329–334.

E. Contreras-Reyes, J. Jara, I. Grevemeyer, S. Ruiz, D. Carrizo, Abrupt change in the dip of the subducting plate beneath north Chile, Nature Geoscience 5 (2012) 342.

B. Delouis, M. Pardo, D. Legrand, T. Monfret, The Mw 7.7 Tocopilla earthquake of 14 November 2007 at the southern edge of the northern Chile seismic gap: rupture in the deep part of the coupled plate interface, Bulletin of the Seismological Society of America 99 (2009) 87–94.

S. Ruiz, M. Metois, A. Fuenzalida, J. Ruiz, F. Leyton, R. Grandin, C. Vigny, R. Madariaga, J. Campos, Intense foreshocks and a slow slip event preceded the 2014 Iquique Mw 8.1 earthquake, Science (2014) 1256074.

C. Sippl, B. Schurr, G. Asch, J. Kummerow, Seismicity structure of the northern Chile forearc from 100,000 double-difference relocated hypocenters, Journal of Geophysical Research: Solid Earth 123 (2018)

4063–4087.
F. Waldhauser, W. L. Ellsworth, A double-difference earthquake location algorithm: Method and application to the northern Hayward fault, California, Bulletin of the seismological society of America 90 (2000) 1353–1368.
S. Hainzl, C. Sippl, B. Schurr, Linear relationship between aftershock productivity and seismic coupling in the Northern Chile subduction zone, Journal of Geophysical Research: Solid Earth 124 (2019) 8726–8738.
J. Feder, Fractals, Springer Science & Business Media, 2013.
P. Toledo, Earthquake Distribution Law Under Small-Strain Steady-Dissipation Conditions at Northern Chile, 2021. URL: https://doi.org/10.5281/zenodo.5546655. doi:10.5281/zenodo.5546655.
M.-A. Branch, T. Coleman, Y. Li, A subspace, interior, and conjugate gradient method for large-scale bound-constrained minimization problems, SIAM Journal on Scientific Computing 21 (1999) 1–23.
B. Efron, R. J. Tibshirani, An introduction to the bootstrap, CRC press, 1994.
C. Vigny, A. Socquet, S. Peyrat, J.-C. Ruegg, M. Métois, R. Madariaga, S. Morvan, M. Lancieri, R. Lacassin, J. Campos, D. Carrizo, M. Bejar-Pizarro, S. Barrientos, R. Armijo, C. Aranda, M. Valderas-Bermejo, I. Ortega, F. Bondoux, S. Baize, H. Lyon-Caen, A. Pavez, J.-P. Vilotte, M. Bevis, B. Brooks, R. Smalley, H. Parra, J.-C. Baez, M. Blanco, S. Cimbaro, E. Kendrick, The 2010 Mw 8.8 Maule megathrust earthquake of Central Chile, monitored by GPS, Science 332 (2011) 1417–1421.
S. Ruiz, E. Klein, F. del Campo, E. Rivera, P. Poli, M. Metois, V. Christophe, J. C. Baez, G. Vargas, F. Leyton, et al., The seismic sequence of the 16 September 2015 Mw 8.3 Illapel, Chile, earthquake, Seismological Research Letters 87 (2016) 789–799.
S. Ruiz, R. Madariaga, Historical and recent large megathrust earthquakes in Chile, Tectonophysics 733 (2018) 37–56.
M. Métois, A. Socquet, C. Vigny, D. Carrizo, S. Peyrat, A. Delorme, E. Maureira, M.-C. Valderas-Bermejo, I. Ortega, Revisiting the North Chile seismic gap segmentation using GPS-derived interseismic coupling, Geophysical Journal International 194 (2013) 1283–1294.
C. Valenzuela-Malebrán, S. Cesca, J. López-Comino, M. Zeckra, F. Krüger, T. Dahm, Source mechanisms and rupture processes of the Jujuy seismic nest, Chile-Argentina border, Journal of South American Earth Sciences 117 (2022) 103887.
U.S. Geological Survey, Earthquake Lists, Maps, and Statistics, accessed Oct/21, 2021. URL: https://www.usgs.gov/natural-hazards/earthquake-hazards/lists-maps-and-statistics.
S. G. Ferraes, Test of Poisson process for earthquakes in Mexico city, Journal of Geophysical Research 72 (1967) 3741–3742.
A. Poulos, M. Monsalve, N. Zamora, J. C. de la Llera, An updated recurrence model for chilean subduction seismicity and statistical validation of its Poisson nature, Bulletin of the Seismological Society of America 109 (2019) 66–74.
S. Janićević, L. Laurson, K. J. Måløy, S. Santucci, M. J. Alava, Interevent correlations from avalanches hiding below the detection threshold, Physical review letters 117 (2016) 230601.
J. Ruegg, J. Campos, R. Armijo, S. Barrientos, P. Briole, R. Thiele, M. Arancibia, J. Canuta, T. Duquesnoy, M. Chang, et al., The Mw=8.1 Antofagasta (North Chile) earthquake of July 30, 1995: first results from teleseismic and geodetic data, Geophysical Research Letters 23 (1996) 917–920.
M. Chlieh, J. De Chabalier, J. Ruegg, R. Armijo, R. Dmowska, J. Campos, K. Feigl, Crustal deformation and fault slip during the seismic cycle in the North Chile subduction zone, from GPS and InSAR observations, Geophysical Journal International 158 (2004) 695–711.
U. Frisch, G. Parisi, Fully developed turbulence and intermittency, New York Academy of Sciences, Annals 357 (1980) 359–367.
T. Hirata, M. Imoto, Multifractal analysis of spatial distribution of microearthquakes in the Kanto region, Geophysical Journal International 107 (1991) 155–162.
C. Hooge, S. Lovejoy, D. Schertzer, S. Pecknold, J.-F. Malouin, F. Schmitt, Mulifractal phase transitions: the origin of self-organized criticality in earthquakes, Nonlinear Processes in Geophysics 1 (1994) 191–197.
D. Comte, A. Cisternas, L. Dorbath, J. Campos, J.-P. Ampuero, Multifractal analysis of the 1995 Antofagasta, northern Chile earthquake, in: Fourth ISAG, volume 04, Goettingen, Germany, 1999.
D. Pastén, D. Comte, ultifractal analysis of three large earthquakes in Chile: Antofagasta 1995, Valparaiso 1985, and Maule 2010, Journal of seismology 18 (2014) 707–713.
A. Scott, Encyclopedia of nonlinear science, Routledge, 2006.
C. Meneveau, K. Sreenivasan, The multifractal nature of turbulent energy dissipation, Journal of Fluid Mechanics 224 (1991) 429–484.
M. Bottiglieri, C. Godano, On-off intermittency in earthquake occurrence, Physical Review E 75 (2007) 026101.
L. Telesca, V. Cuomo, V. Lapenna, M. Macchiato, Intermittent-type temporal fluctuations in seismicity of the Irpinia (southern Italy) region, Geophysical research letters 28 (2001) 3765–3768.
Y. Abe, N. Kato, Intermittency of earthquake cycles in a model of a three-degree-of-freedom spring-block system, Nonlinear Processes in Geophysics 21 (2014) 841–853.
R. Benzi, I. Castaldi, F. Toschi, J. Trampert, Self-similar properties of avalanche statistics in a simple turbulent model, Philosophical Transactions of the Royal Society A: Mathematical, Physical and Engineering Sciences 380 (2022) 20210074.
K. Obara, A. Kato, Connecting slow earthquakes to huge earthquakes, Science 353 (2016) 253–257.
G. Rogers, H. Dragert, Episodic tremor and slip on the Cascadia subduction zone: The chatter of silent slip, science 300 (2003) 1942–1943.
K. Shimazaki, T. Nakata, Time-predictable recurrence model for large earthquakes, Geophysical Research Letters 7 (1980) 279–282.
C. Vigny, E. Klein, The 1877 megathrust earthquake of North Chile two times smaller than thought? A review of ancient articles, Journal of South American Earth Sciences 117 (2022) 103878.
J. Jara, A. Socquet, D. Marsan, M. Bouchon, Long-term interactions between intermediate depth and shallow seismicity in north chile subduction zone, Geophysical Research Letters 44 (2017) 9283–9292.
F. Omori, On the after-shocks of earthquakes, J. Coll. Sci., Imp. Univ., Japan 7 (1894) 111–200.
T. Utsu, Y. Ogata, R. S. Matsu'ura, The centenary of the Omori formula for a decay law of aftershock activity, Journal of Physics of the Earth 43 (1995) 1–33.
G. S. Golitsyn, Place of the Gutenberg-Richter law among other statistical laws of nature, Vychislitel'naya Seysmologiya 32 (2001) 119–137.
N. A. Heckert, J. J. Filliben, C. M. Croarkin, B. Hembree, W. F. Guthrie, P. Tobias, J. Prinz, Handbook 151: NIST/SEMATECH e-Handbook of Statistical Methods, NIST, 2002. doi:10.18434/M32189.
Y. Ogata, S. Toda, Bridging great earthquake doublets through silent slip: On- and off-fault aftershocks of the 2006 Kuril Island subduction earthquake toggled by a slow slip on the outer rise normal fault of the 2007 great earthquake, Journal of Geophysical Research B06318 (2010).

Appendix

A. Omori law and interevent-times

In the Earth crust, given an observation time t is natural to suppose that the probability distribution $n(t)$ be different from $n(s)$ taken from a different observation time s, just because the total number of events update is due. Losing full generality, we might keep the Poisson distribution but the parameter $\nu(t)$ will be different for different time lapses.

Within an aftershock sequence, the dimensionless seismic rate is given by:

$$\frac{d\nu}{dt} = \frac{K}{(C+t)^p}, \tag{19}$$

with K, C and p real values. It was first recognized by Omori (1894) when $p = 1$ and later generalized by Utsu et al. (1995) for real positive values $p > 0$. This case has non-stationary increments, therefore is a non-homogeneous Poisson process example. The incomplete similarity solution where $C = 0$, that is the asymptotic regime far enough from a mainshock and at the same time distant from quiescence is a power-law with non-integer exponent derived by Golitsyn (2001) as a self-similar solution of the second kind.

When aftershocks are distributed according to Omori rate in equation (19), it is no longer possible to obtain a formula for the interevent-times distribution, but we can write an expression for $T(t_k|t_{k-1})$ the conditional cumulative distribution, that is given an event taking place at t_{k-1} the cumulative distribution for the next time t_k is:

$$\begin{aligned} T(t_k|t_{k-1}) &= 1 - \exp\left(-\nu(t_k)\right), \\ &= 1 - \exp\left(\frac{K}{1-p}\left[(t_{k-1}-t_k)^{1-p} - {t_{k-1}}^{1-p}\right]\right), \end{aligned}$$

we should note that if $k = 1$ the cumulative distribution represents the beginning of an aftershock sequence and it so happens that t_1 follows a Weibull distribution, we must remark that for later events this is not true anymore (Heckert et al., 2002). More advanced cases where the interevent-times are not exponentially distributed are called *renewal processes,* (see for example the ETAS model of seismicity Ogata and Toda, 2010).

B. Collapse curves process

Let us show how the collapse process occurs. In Figure 9 it is shown a situation where there is no collapse for the curves of renormalized released energy. It is possible to appreciate how families of curves for different proper sizes ℓ, are separated between each other, i.e. there's no scaling function ϕ^* that can account for this situation. Nonetheless, it can be appreciated a certain relation for the longer return periods (in colors), as also for the magnitudes (marker sizes)

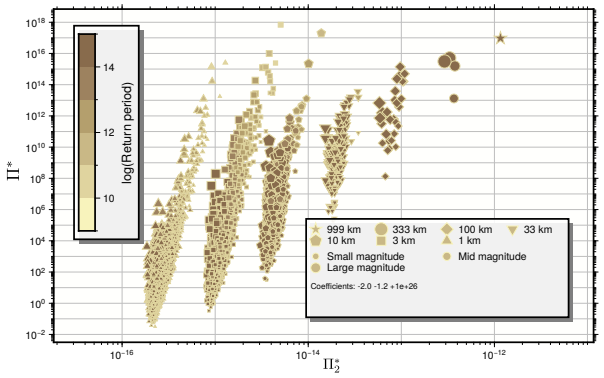

Figure 9: Uncollapsed renormalized energy versus renormalized stress drops. At a fixed point, the scaling function ϕ^* shows a definite shape, frequently a power law. We illustrate a situation where collapsing is not achieved, exponents are $\alpha = -2$, $\alpha_1 = -1.2$ and $\kappa = 1 \times 10^{26}\,\mathrm{Jm}^{-2}$. As shown, exponents do not represent a physically sound law as no scaling function might account for this scenario.

CRediT authorship contribution statement

Patricio A. Toledo: Conceptualization of this study, Methodology, Software. **Cristián Siegel:** Conceptualization of this study, Methodology, Software. **Sebastián Riquelme:** Conceptualization of this study, Methodology, Software. **Raúl Madariaga:** Conceptualization of this study, Methodology, Software. **Jaime Campos:** Conceptualization of this study, Methodology, Software.